

## Lateral multiple scattering of energetic ions in very thin targets: $Z_1$ oscillations

H. Knudsen, F. Besenbacher, J. Heinemeier, and P. Hvelplund

*Institute of Physics, University of Aarhus, DK-8000 Aarhus C, Denmark*

(Received 12 February 1976)

We report measurements of lateral multiple scattering of 15–60-keV ions with atomic number from 6 to 82 on xenon targets of reduced thickness  $0.01 < \tau < 0.17$ . Significant deviations from the scaling properties inherent in current multiple-scattering theory are observed. The widths of the multiple-scattering distributions are not strictly proportional to the reciprocal ion energy, and they oscillate heavily with ion atomic number. These oscillations are similar to those found in electronic stopping power.

### I. INTRODUCTION

Angular multiple scattering of heavy energetic ions has been extensively investigated both theoretically<sup>1–3</sup> and experimentally.<sup>4–12</sup> These investigations were made not only because multiple scattering is of practical importance in the design of accelerators and in experiments involving accelerated beams, but also because knowledge of the collision processes (e.g., the interatomic potential) can be obtained from the measured angular distributions.

The thinner the target, the more sensitive are multiple-scattering distributions to the interaction potential at large distances. Because of problems with suitable confinement of gaseous targets, measurements of angular distributions have, until now, been limited to self-supporting-foil targets. This means that for target thicknesses smaller than those obtainable for self-supporting foils, angular multiple scattering has not been investigated. (See, however, Ref. 13.)

Recently Marwick and Sigmund<sup>14</sup> showed that lateral multiple-scattering distributions are practically identical to angular distributions except for certain scaling factors and that they therefore contain the same information. As lateral scattering distributions can easily be measured for gaseous targets,<sup>15,16</sup> this made it possible to investigate multiple-scattering phenomena for very small target thicknesses, where the sensitivity to the interaction potential at large internuclear distances is very pronounced.

This paper reports on measurements of lateral multiple-scattering distributions for 15–60-keV ions, with atomic numbers from 6 to 82, scattered on xenon. The reduced target thickness  $\tau$  is in the region from 0.01 to 0.17.<sup>16(a)</sup>

### II. THEORY

When an originally well-collimated beam penetrates matter, the ions are scattered. The central part of the resulting angular distribution consists

of ions having suffered many weak collisions, and it is therefore called the angular multiple-scattering distribution. The angular scattering of the beam during its passage of an extended target creates a spatial distribution of the beam inside the target, the so-called lateral multiple-scattering distribution.

The theory of multiple scattering of energetic ions has been advanced by Meyer<sup>2</sup> and Sigmund and Winterbon<sup>3</sup> and is based on the atomic-collision model of Lindhard *et al.*<sup>17</sup> In this model, the differential elastic-scattering cross section between the ion ( $Z_1, M_1, E$ ) and the target atom ( $Z_2, M_2$ ) is given as

$$d\sigma = -\pi a^2 f(t^{1/2}) dt/2t^{3/2}, \quad (1)$$

where

$$t^{1/2} = \epsilon \sin \frac{1}{2} \theta, \quad (2)$$

$$\epsilon = [M_2/(M_1 + M_2)] aE/Z_1 Z_2 e^2, \quad (3)$$

$$a = 0.8853 a_0 (Z_1^{2/3} + Z_2^{2/3})^{-1/2}. \quad (4)$$

Here  $\theta$  is the center-of-mass scattering angle and  $a_0$  is the Bohr radius.  $f(t^{1/2})$  is a reduced differential-scattering cross section computed numerically from the Thomas-Fermi (TF) or the Lenz-Jensen (LJ) interatomic potential. When only a limited  $t^{1/2}$  interval is considered, the real interatomic potential can be approximated by a power-law potential,

$$V(r) \propto r^{-1/m}. \quad (5)$$

Then

$$f(t^{1/2}) = \lambda_m (t^{1/2})^{1-2m}, \quad (6)$$

where  $\lambda_m$  is a constant.

The model of Lindhard *et al.*<sup>17</sup> assumes classical trajectories for the colliding particles. This approximation is appropriate when

$$\kappa = 2 Z_1 Z_2 e^2 / \hbar v > 1 + (p/a)^2 \quad (7)$$

where  $v$  is the velocity of the ion and  $p$  is the impact parameter.

The calculations of Sigmund and Winterbon<sup>3</sup> are based on the following assumptions:

- (a) Random homogeneous distribution of scattering centers in space.
- (b) Binary collision events with azimuthal symmetry of scattering.
- (c) Negligible energy losses.
- (d) Small scattering angles in the center-of-mass system.

In the notation of Sigmund and Winterbon, the absolute intensity of the angular distribution is written

$$f_1(\tau, \bar{\alpha}) \bar{\alpha} d\bar{\alpha}. \quad (8)$$

Here  $\tau$  is the reduced target thickness,

$$\tau = \pi a^2 N x, \quad (9)$$

where  $Nx$  is the product of target atomic density and length, and

$$\bar{\alpha} = (Ea/2 Z_1 Z_2 e^2) \alpha \quad (10)$$

is a reduced scattering angle proportional to the laboratory scattering angle  $\alpha$ .  $f_1(\tau, \bar{\alpha})$ , calculated for the TF and the LJ potentials, is tabulated in Refs. 2 and 3, where also the reduced half width at half-maximum (HWHM)  $\bar{\alpha}_{1/2}$  can be found.  $\bar{\alpha}_{1/2}$  depends on  $\tau$  only. For power-law potentials it can be shown that

$$\bar{\alpha}_{1/2} = C_m \tau^{1/2m}. \quad (11)$$

For  $\tau < 0.07$ , the HWHM's corresponding to the TF potential can be approximated by Eq. (11), with  $C_m = 1.05$  and  $m = 0.311$ , whereas for the LJ potential,  $C_m = 3.45$  and  $m = 0.191$ .

Within the above framework, Marwick and Sigmund<sup>14</sup> expressed the absolute intensity of the lateral multiple-scattering distribution as

$$g_1(\tau, \bar{\rho}) \bar{\rho} d\bar{\rho}, \quad (12)$$

where the reduced lateral spread

$$\bar{\rho} = (\tau/x) (Ea/2 Z_1 Z_2 e^2) \rho \quad (13)$$

is proportional to the absolute lateral spread  $\rho$ . As an important result, they found that to a good approximation  $g_1(\tau, \bar{\rho})$  is given by  $f_1(\tau, \bar{\alpha})$  through the following scaling law:

$$g_1(\tau, \bar{\rho}) = (\Gamma/\tau)^2 f_1(\tau, \Gamma \bar{\rho}/\tau). \quad (14)$$

$\Gamma$  is a slowly decreasing function of  $\tau$ , calculated numerically from TF and LJ potentials in Ref. 14. For power-law potentials,

$$\Gamma_m = (1 + 2m)^{1/2m}. \quad (15)$$

From Eq. (14) it can be seen that

$$\bar{\rho}_{1/2} = (\tau/\Gamma) \bar{\alpha}_{1/2}, \quad (16)$$

and in particular for power-law potentials,

$$\bar{\rho}_{1/2} = (C_m/\Gamma_m) \tau^{1+1/2m}. \quad (17)$$

For scattering which can be described by Eq. (1) both  $\bar{\rho}_{1/2}$  and  $\bar{\alpha}_{1/2}$  are dependent on  $\tau$  only. Thus all experimental values of  $\bar{\rho}_{1/2}$  should lie on one universal curve as a function of  $\tau$ , independent of the values of  $Z_1$ ,  $Z_2$ , and  $E$ . For the power-law potentials, it is found from Eqs. (13) and (17) that

$$\rho_{1/2} \propto E^{-1} P^{1/2m} x^{1+1/2m}, \quad (18)$$

where  $\rho_{1/2}$  is the measured HWHM and  $P$  the target pressure.

A comparison between measured values of  $\bar{\rho}_{1/2}(\tau)$  and theoretical predictions supplies information on  $f(t^{1/2})$  and consequently on the interatomic potential. For example, the value of  $m$  in Eq. (6) can be found through Eq. (17). This information applies to a limited  $t^{1/2}$  range, depending on the value of  $\tau$ . Generally, the angular deflection in the dominant type of collision creating the central part of a given multiple-scattering distribution is of the order of the HWHM  $\alpha_{1/2}$ . If  $(t^{1/2})^*$  is defined as the value of  $t^{1/2}$  for such a collision, then this fact can be expressed, because of assumption (d) above, as

$$(t^{1/2})^* = R(\tau) \bar{\alpha}_{1/2}, \quad (19)$$

where  $R(\tau) \approx 1$ .

For  $\tau < 0.07$ , Sigmund<sup>18</sup> finds the value of  $R(\tau)$  to be 2.2 for the TF potential and  $R(\tau) = 2.8$  for the LJ potential. Calculations by Schöffler<sup>9</sup> indicate that for  $1 < \tau < 20$ , the value of  $R(\tau)$  is close to 1 for both TF and LJ potentials. The "effective" reduced scattering parameter  $(t^{1/2})^*$  is indicated in Fig. 1 for the TF and LJ potentials. Also shown in the figure, in units of  $a$ , are the values  $(p/a)^*$  of the impact parameter  $p$  corresponding to  $(t^{1/2})^*$ . The curves marked " $\bar{\alpha}_{1/2}(\text{TF})$ " and " $\bar{\alpha}_{1/2}(\text{LJ})$ " apply for large values of  $\tau$ , while for small  $\tau$  the curves marked " $2.2\bar{\alpha}_{1/2}(\text{TF})$ " and " $2.8\bar{\alpha}_{1/2}(\text{LJ})$ " apply. In our measurements,  $\tau$  is in the range from 0.01 to 0.17, and the measured HWHM's  $\bar{\rho}_{1/2}$  are better described by the LJ than by the TF theoretical curve. Hence the information obtained from our results concerns collisions with  $6 \times 10^{-5} \leq t^{1/2} \leq 6 \times 10^{-2}$ , corresponding to the impact-parameter interval of  $2.5a \leq p \leq 17a$ .

For a comparison between the theoretically predicted results and those obtained experimentally, we shall discuss to what extent the conditions on which the theory is based are fulfilled. It is possible to use classical mechanics, since Eq. (7) is satisfied in our case. This is easily seen by using the effective impact parameters of Fig. 1. Conditions (a) and (b) above are clearly met for a xenon-gas target, and (c) and (d) are valid as will be discussed later. Furthermore, the statistical

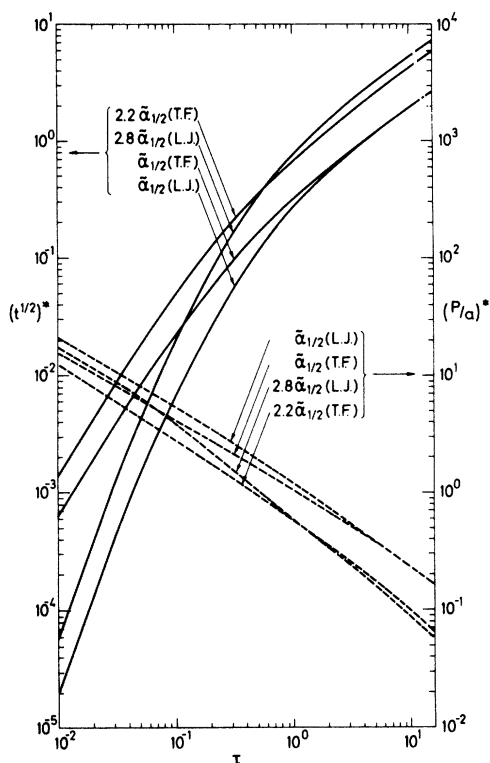


FIG. 1. Impact parameter and  $t^{1/2}$  value corresponding to the collisions most effective for the creation of the multiple-scattering distributions, shown as function of the reduced thickness  $\tau$ , according to Eq. (19).

description of the atoms and the unified model of Lindhard *et al.*<sup>17</sup> should apply. As stated in Ref. 17, this is the case for  $p \lesssim 5a$ . For larger  $p$ , deviations from the  $Z_1, Z_2$  scaling are expected. The energy scaling, on the other hand, is not based on the statistical description but rather on the condition that the deflections are caused by an energy-independent potential. Therefore it is expected to be fulfilled except perhaps for the largest  $p$  values dealt with here. In conclusion, the theoretical results mentioned in this section should be valid for the largest  $\tau$  values, whereas for the smaller  $\tau$  values, they are used only as a

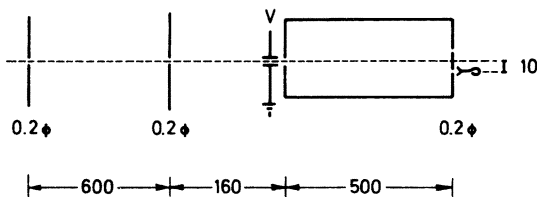


FIG. 2. Experimental setup. All dimensions are in millimeters. The drawing is not to scale.

convenient framework for representing the experimental data.

### III. EXPERIMENTAL

The experimental setup is shown schematically in Fig. 2, with the dimensions given in millimeters. The singly charged ion beam is collimated by two  $\sim 0.2$ -mm-diam apertures 600 mm apart. It then passes through a deflection system consisting of two pairs of electrostatic deflection plates, of which the first is for vertical deflection and the second (not shown) is for horizontal deflection. The beam is then lead through an entrance aperture into a 500-mm-long gas cell, where it is scattered on the target gas. Behind the  $\sim 0.2$ -mm-diam exit aperture placed 10 mm below the beam axis is a channeltron which detects all particles passing through this aperture.

After their passage of the target gas, the ions exhibit a lateral distribution, which is measured by sweeping the beam across the exit aperture by means of the vertical deflection plates. Output from the channeltron is fed through standard electronics to a multichannel analyzer in such a way that the pulses are counted in a channel, the number of which is proportional to the momentary value of the sweeping voltage.

In this way, the lateral distribution appears directly as a spectrum in the multichannel analyzer. The beam is swept across the exit aperture approximately 100 times with a frequency of  $\sim 0.1$  Hz, which is not correlated to any accelerator-based frequency in beam intensity. Thus the beam intensity is averaged in time and no normalization is needed.

To find the conversion factor between channel number and the position  $\rho$  in the lateral distribution, we used a number of holes placed vertically, 10 mm apart, above the exit aperture. Without target gas, the beam is swept across these holes (only one is indicated in Fig. 2), and the observed current, converted to counts, is lead to the multichannel analyzer. Several narrow peaks are obtained, and the distance of 10 mm between them is equivalent to the difference in channel number. The system is found to be linear to within 1%. Separability of spatial variables does not apply to the non-Gaussian distributions, and it is therefore important to scan through their maximum to obtain the true profile. This was achieved by careful adjustment of the horizontal-deflection voltage, which was subsequently checked at regular intervals.

The target was pure xenon gas, lead from a reservoir through a needle valve into the gas cell. The pressure in this cell was measured with a

Pirani gauge calibrated against a membrane manometer. Using Eq. (9), we find that

$$\tau = 0.517a^2P, \quad (20)$$

where  $a$  is measured in Å and  $P$  in mTorr.

Prior to a comparison between the measured distributions and the theoretical results, two corrections should be considered:

(1) The ions always lose a small amount of energy during their passage through the target. The average energy during passage is therefore close to

$$E = E_0 - \frac{1}{2} \Delta E. \quad (21)$$

$E_0$  is the incident energy and  $\Delta E = \Delta E_e + \Delta E_n^*$ , where  $\Delta E_e$  is the electronic energy loss and  $\Delta E_n^*$  is the energy loss owing to soft nuclear collisions suffered by the ions found in the central part of the multiple-scattering distributions. By means of formula (A1) of Ref. 19, we have calculated  $\Delta E_n^*$  to be less than 1.5% in all cases, and  $\Delta E_e$  was found from Lindhard *et al.*<sup>20</sup> to be less than 4.5%. Thus the energy-loss correction is only a few percent and is therefore negligible.

(2) We have to correct the measured distributions for the finite resolution of the apparatus. This is due to the fact that the incoming beam has a finite radius  $r_B$  and the exit aperture a finite radius  $r_C$ . As found by Sidenius and Andersen,<sup>15</sup> the corrected HWHM is approximated by

$$\rho_{1/2} = [1 - K(m)(r/\rho'_{1/2})^2] \rho'_{1/2}, \quad (22)$$

where  $\rho'_{1/2}$  is the measured value and

$$r = (r_B^2 + r_C^2)^{1/2}. \quad (23)$$

$K(m)$  is given in Ref. 15. The actual value of  $m$  to be used in Eq. (22) will be discussed in Sec. IV. From the distribution obtained by sweeping the beam without target gas,  $r$  was obtained as the HWHM and was found to be  $r = 0.095$  mm. The magnitude of the correction in Eq. (22) was found to be less than a few percent for most of the measured distributions, but in a few cases it reached 25%.

For our measurements of lateral-distribution HWHM's, the dominant source of random error (5%–15%) originates from counting statistics. The systematic error is believed to be less than 5%.

#### IV. RESULTS

An example of an experimental distribution is shown in Fig. 3. It was obtained with 50-keV Ar  $\rightarrow$  Xe and  $\tau = 0.036$ . Also shown is a theoretical distribution obtained by using Eq. (14) from a power potential with  $m = 0.24$  (see below). The peak value of the theoretical distribution was

normalized to the experimental one. The agreement is excellent.

Figure 4 shows measured reduced HWHM's for 50-keV Ar  $\rightarrow$  Xe as a function of reduced target thickness compared to the theoretical curves calculated from the TF and LJ potentials. Also indicated is an example of the magnitude of the energy loss, where  $\Delta E = \Delta E_n^* + \Delta E_e$ . This was calculated from the theory of Lindhard *et al.*<sup>17,20</sup> and Hvelplund *et al.*<sup>19</sup> It is noted that the experimental points all fall very close to the straight line

$$\bar{\rho}_{1/2} = 0.635\tau^{3.092}, \quad (24)$$

which corresponds to the HWHM calculated by using a power potential with  $m \approx 0.24$ . From Fig. 3 it is seen that this potential describes not only the  $\tau$  dependence of  $\bar{\rho}_{1/2}$  but also the shape of the distributions.

Figure 5 shows measured reduced HWHM's for many different 50-keV ions ( $6 \leq Z_1 \leq 82$ ) scattered on xenon gas. It is noticed that the LJ curve is in better agreement with the experimental points than is the TF curve. As for the Ar  $\rightarrow$  Xe case, the best straight lines can be found for each  $Z_1$  value, and from there the power-potential parameters  $\Gamma_m$ ,  $C_m$ , and  $m$  appearing in Eqs. (6), (11), and (17) can be determined. Some of these are given in Table I together with the parameters belonging to the line that represents the mean trend of all of the points,

$$\bar{\rho}_{1/2} = 1.73\tau^{3.47}. \quad (25)$$

The choice of  $K(m)$  in Eq. (22) is based on  $m$  values found in this way.

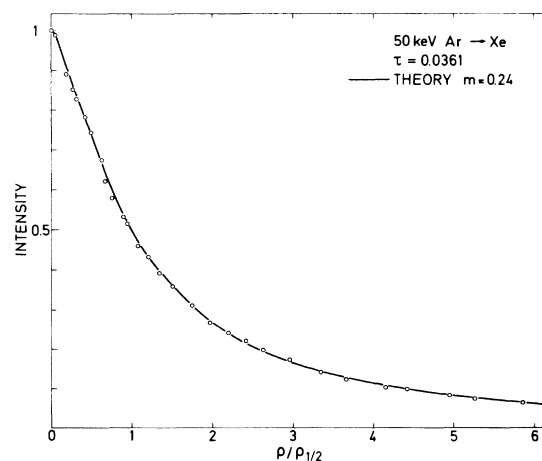


FIG. 3. Experimental lateral-scattering distribution for 50-keV Ar on Xe with  $\tau = 0.0361$ . Also shown is a theoretical distribution corresponding to a power-law potential with  $m = 0.24$ . The two distributions were normalized at the center of the distributions.

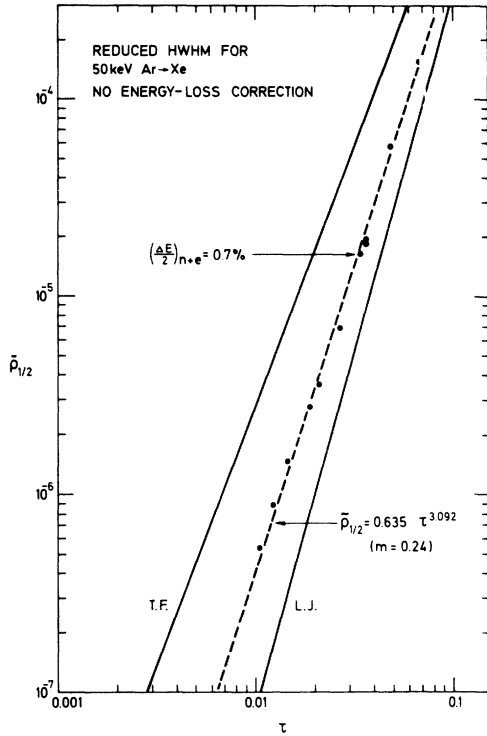


FIG. 4. Experimental reduced HWHM's for 50-keV Ar scattered on Xe as function of reduced target thickness  $\tau$ . Also shown are an average experimental curve and the curves belonging to TF and LJ potentials.

The scatter of the points in Fig. 5 is large. However, this is not due to experimental uncertainty, as can be concluded from an examination of Fig. 4 and from the stated uncertainties in Sec. III.

To find the reason for the scatter, we investigated the quantity  $\bar{\rho}_{1/2}(Z_1)$  for fixed  $\tau$  values. For this purpose, we measured a number of distributions at fixed target pressure ( $P \approx 6.50$  mTorr) by varying  $Z_1$ . According to Eq. (20), this corresponds to  $\tau$  values near 0.033. By means of Eq. (25), the  $\bar{\rho}_{1/2}$  values were interpolated to  $\tau = 0.033$  according to the formula

$$\bar{\rho}_{1/2, \tau=0.033} = \bar{\rho}_{1/2} / (\tau/0.033)^{3.47}. \quad (26)$$

Since all of the actual  $\tau$  values are close to 0.033, the result of this interpolation is not changed perceptibly if, instead of the mean exponent 3.47, the actual values found from Fig. 5 for given  $Z_1$  are used.

The result of the interpolation is shown in Fig. 6, where for  $Z_1 \leq 51$ , the values of  $\bar{\rho}_{1/2}$  are plotted as a function of  $Z_1$ . For C, O, S, Cl, Ar, Fe, and Cu, more than one distribution was measured. The values of  $\bar{\rho}_{1/2}$  calculated from TF and LJ potentials are shown. As mentioned in Sec. II, these

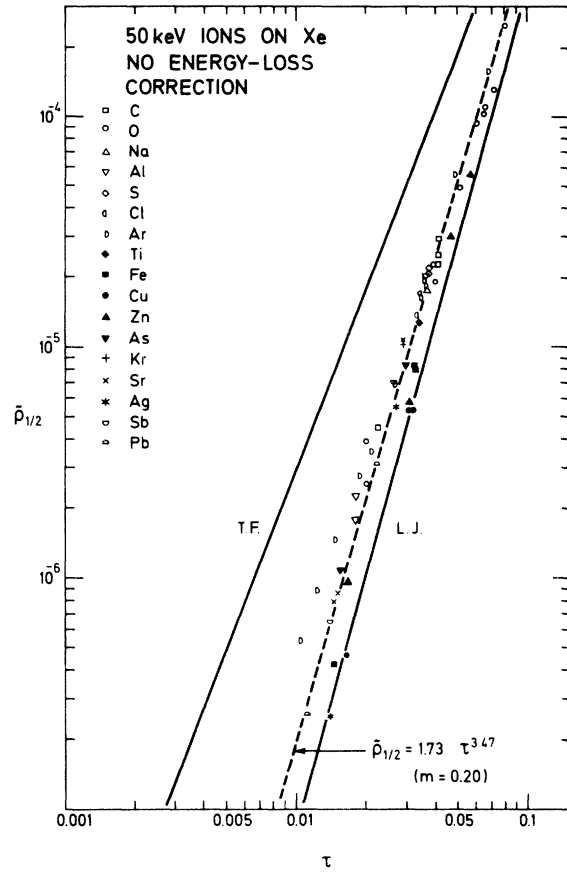


FIG. 5. Measured reduced HWHM's of lateral distributions of many different 50-keV ions scattered on Xe as function of  $\tau$ . Also shown is the straight line common to all of the points.

TABLE I. Power-law-potential parameters found from the  $\tau$  dependence of the reduced HWHM of 50-keV Ar, O, and Cu ions scattered on Xe at  $\tau < 0.07$ . Also given are the parameters for the curve corresponding to the average trend of all of our measured HWHM's at  $\tau < 0.07$  and the parameters corresponding to the results obtained from TF and LJ potentials.

	$\Gamma_m$	$C_m$	$m$
TF	2.176	1.05	0.311
Ar	2.26	1.41	0.24
O	2.29	1.89	0.22
$\langle Z_1 \rangle$	2.32	4.01	0.20
Cu	2.33	3.45	0.19
LJ	2.333	3.45	0.191

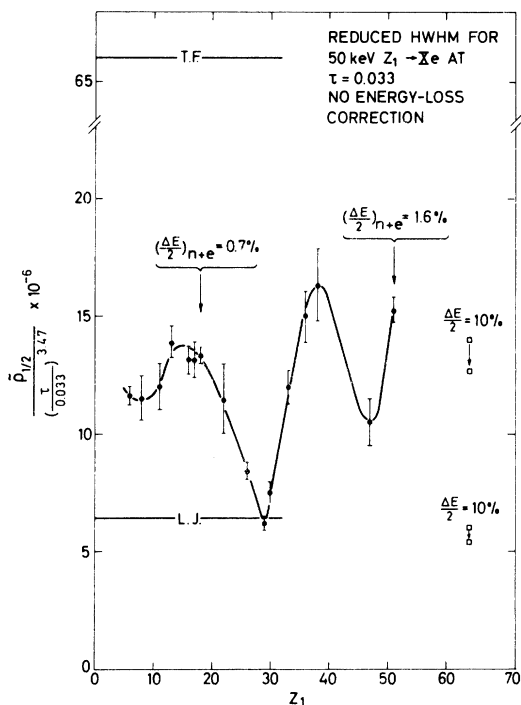


FIG. 6. Reduced HWHM's of lateral multiple-scattering distributions measured for many different ions on Xe at the reduced target thickness  $\tau = 0.033$  as a function of ion atomic number  $Z_1$ . Also indicated are the theoretical values calculated from LJ and TF potentials. (Note the broken axis).

do not depend on  $Z_1$ . (Note the broken axis.)

From a calculation similar to that described in Sec. III, it is found that an upper limit to the energy-loss correction is 1.6%. An energy-loss correction  $\frac{1}{2}\Delta E$  as large as 10% would only move the experimental points as indicated, and thus the energy-loss correction is clearly negligible.

The most remarkable result found from Fig. 6 is that  $\bar{\rho}_{1/2}$  oscillates strongly as a function of  $Z_1$ . There are maxima for  $Z_1 \approx 15$  (P) and 38 (Sr) and minima for  $Z_1 = 8$  (O), 29 (Cu), and 47 (Ag). The amplitude is of the order of 40%.

An alternative representation of the data in Fig. 6 is given in Fig. 7, where the directly measured HWHM's for fixed target-gas pressure ( $\approx 6.50$  mTorr) are plotted as a function of  $Z_1$ . As the actual target-gas pressure deviated by less than a few percent from 6.50 mTorr, the  $\rho_{1/2}$  values have been interpolated in a manner analogous to Eq. (26), i.e., according to Eq. (18), as

$$\rho_{1/2, P=6.50} = \rho_{1/2} / (P/6.50)^{2.47}, \quad (27)$$

where  $P$  is measured in mTorr.

Superimposed on the increasing HWHM as a function of  $Z_1$  are oscillations with the same extrema as those found in Fig. 6. Also shown is the

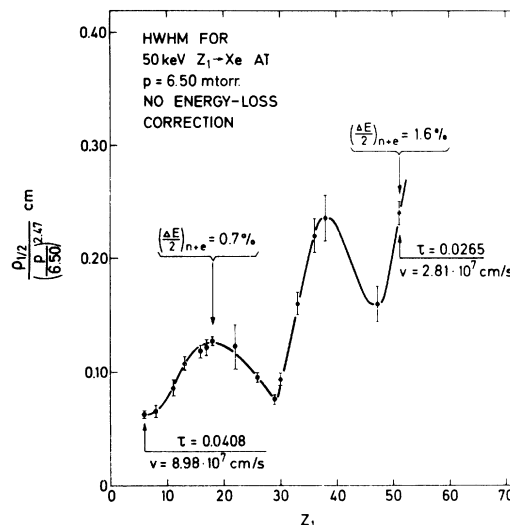


FIG. 7. Measured HWHM's of lateral distributions obtained with many different ions scattered on a Xe target with pressure  $P = 6.50$  mTorr.

$\tau$  interval and the variation in ion velocity  $v$  for fixed energy (50 keV).

The result of a similar analysis of HWHM's for distributions measured with target-gas pressure  $\approx 3.25$  mTorr and resulting  $\tau$  values near 0.017 is shown in Figs. 8 and 9. Owing to the limited number of experimental points, it is difficult to draw a curve, but one observes that the points are somewhat closer to the LJ value than they were at  $\tau = 0.033$ , that the oscillations are relatively larger, and that the same extrema are found.

To present the shape of the measured lateral distributions, we formed the parameter  $I(2\rho_{1/2})/I(0)$ , which is the intensity at twice the HWHM relative to the intensity in the center of the dis-

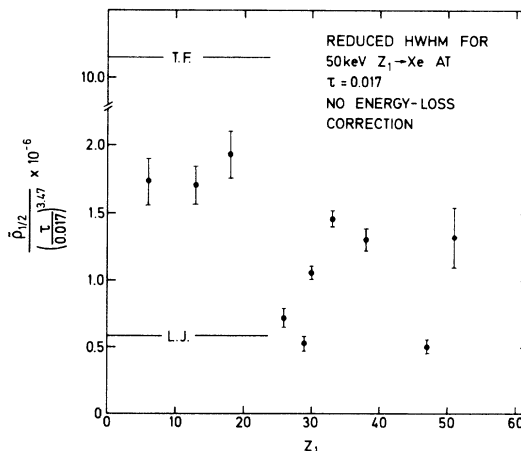


FIG. 8. Experimental results corresponding to those shown in Fig. 6, but here  $\tau = 0.017$ .

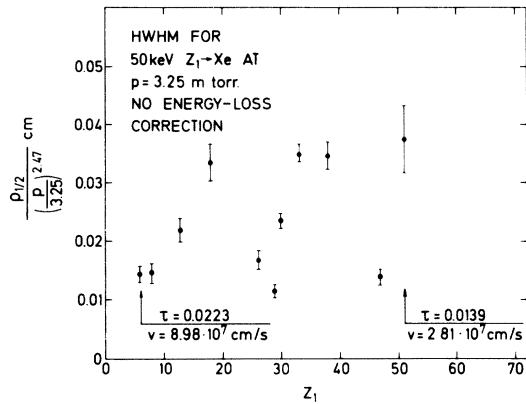


FIG. 9. Experimental results corresponding to those shown in Fig. 7, but measured at a target pressure of 3.25 mTorr.

tribution. For the distributions measured at  $\tau \approx 0.033$ , this parameter is shown in Fig. 10 as a function of  $Z_1$ . Also indicated is the value corresponding to a Gaussian distribution and that found for a power-law potential with  $m = 0.20$ . As was the case for the HWHM's (Fig. 5), this potential describes very well the general trend of the results. The scatter of the points is due partly to experimental uncertainty and partly to the variation of  $I(2\rho_{1/2})/I(0)$  with the power-law-potential parameter  $m$  as given with examples in Table I (see Ref. 3, Fig. 1). In Fig. 10, extrema can be found at  $Z_1 = 29, 38$ , and  $47$ , the same values as those found for the  $\bar{\rho}_{1/2}$  oscillations, but here the relative amplitude is much smaller.

The majority of our measurements were performed with an ion energy of 50 keV. However, a number of distributions were measured for Ar and Cu beams with energies varying from 15 to 60 keV, using a xenon target ( $P \approx 6.50$  mTorr,  $\tau \approx 0.033$ ). Ar and Cu were chosen since they are found in the top and bottom, respectively, of the  $Z_1$  oscillations in HWHM. The directly measured HWHM's are shown in Fig. 11 as a function of energy. According to Eq. (18), they should depend on energy as  $E^{-1}$ , but for argon, the exponent is  $-(1.15 \pm 0.06)$ , while for copper it is  $-(0.88 \pm 0.06)$ . Consequently, the relative amplitude in the oscillations increases with decreasing energy.

#### V. COMPARISON WITH OTHER DATA

To the best of our knowledge, the only existing measurements of multiple scattering of heavy energetic ions on targets with reduced thicknesses as small as those reported here have been performed by Efken *et al.*<sup>13</sup> and by Sidenius and Andersen.<sup>15,16</sup> Efken *et al.* measured angular multiple-scattering distributions of 15-MeV neon and argon

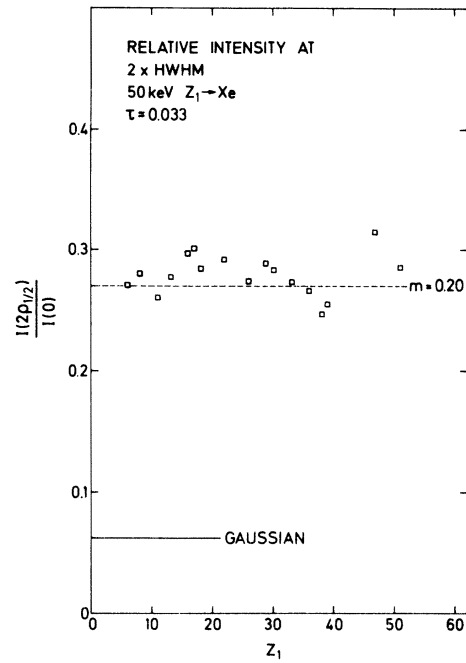


FIG. 10. Intensity at twice the HWHM relative to the intensity at the center of lateral distributions measured for 50-keV ions scattered on Xe targets with reduced target thickness near 0.033. Also shown are the value corresponding to a power-law potential with  $m = 0.20$  and the value belonging to a Gaussian distribution.

scattered on He,  $N_2$ ,  $SF_6$ , and Ar targets with  $0.02 < \tau < 20$ . However, they present the resulting HWHM's for  $0.6 < \tau < 20$  only, the lower limit being given by the finite resolution of their experimental setup. For  $0.6 < \tau < 20$ , their results are in agreement with the theoretical  $\bar{\alpha}_{1/2}(\tau)$  curve. Sidenius and Andersen<sup>16</sup> measured lateral distributions for 50–180-keV H, He, N, Ne, and Ar ions scattered on Ar and  $N_2$  with  $0.4 < \tau < 15$ . They converted their  $\bar{\rho}_{1/2}$  results to  $\bar{\alpha}_{1/2}$  values, using the scaling law [Eq. (16)], and found agreement with the data of Efken *et al.*, so that Eq. (16) has been checked experimentally. Sidenius and Andersen<sup>15</sup> also measured lateral distributions for 20–180-keV ions with  $1 \leq Z_1 \leq 19$  scattered on a xenon target with  $0.07 < \tau < 0.40$ . The results can be directly compared with the present distributions measured at the largest target thicknesses. Figure 12 shows the HWHM's from Ref. 15 together with our results ( $Z_1$  values can be found from Fig. 5, and for  $\tau > 0.08$ , our points were obtained with carbon and oxygen ions). The results shown in Fig. 12 have been corrected for energy loss according to the discussion in Sec. III. Shown in the figure are straight lines (power-law potentials) fitted to the two data sets. For the results of Sidenius and Andersen, the line is given by

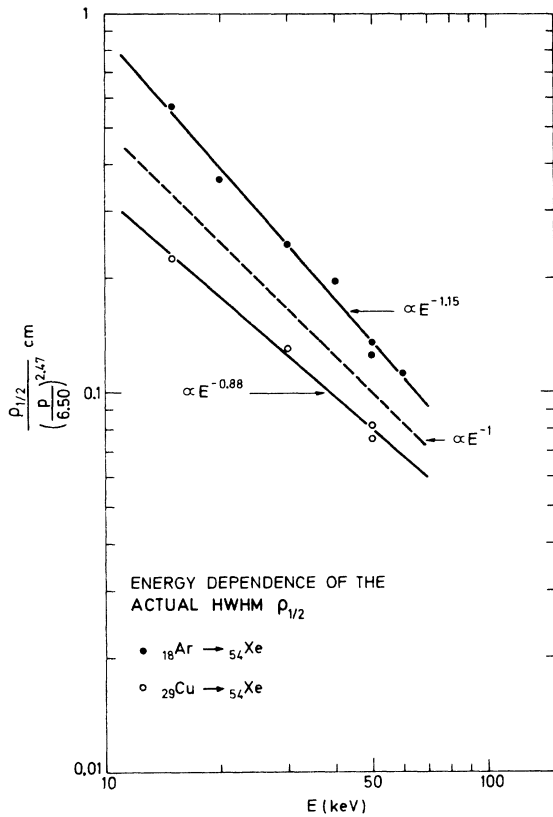


FIG. 11. Directly measured HWHM's  $\rho_{1/2}$  for Ar and Cu ions scattered on a Xe target with target pressure  $P = 6.50$  mTorr (corresponding to  $\tau = 0.035$  for Ar and 0.031 for Cu) as a function of ion energy. Also shown are straight lines calculated from a least-squares-fit method and a dashed line having the slope  $-1$ .

$$\bar{\rho}_{1/2} = 0.22 \tau^{2.5}, \quad (28)$$

corresponding to  $m = 0.33$ . In contrast to the oscillatory behavior of our results, the scatter of their points is due to experimental uncertainty only. It is noticed that at large  $\tau$ , our points asymptotically approach Eq. (28). The reason for the rather large discrepancies at  $\tau \approx 0.08$  is not known.

Sidenius and Andersen<sup>15</sup> find that the  $E^{-1}$  scaling predicted by theory is valid in their  $\tau$  range.

## VI. DISCUSSION

To discuss existing experimental results for angular and lateral multiple scattering of energetic atomic projectiles, it is useful to look at three  $\tau$  intervals:

(1) For  $\tau \approx 0.4$ , the collisions that are effective for the creation of the distributions are described by  $t^{1/2}$  values larger than  $10^{-1}$ . Here, the theoretical results of Refs. 2, 3, and 14 calculated for the LJ or TF potential agree with the experimental

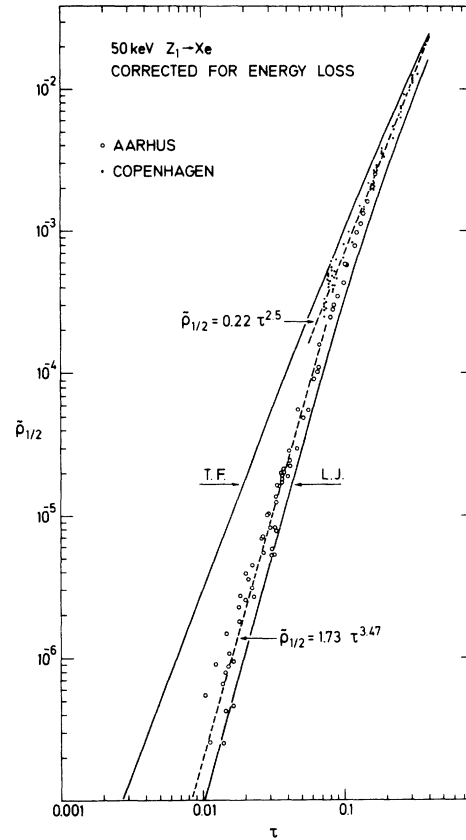


FIG. 12. Comparison between the results of Sidenius and Andersen (Ref. 15) ("Copenhagen") and our measured reduced HWHM's ("Aarhus").

data. The  $Z_1$ ,  $Z_2$ , and  $E$  scaling is fulfilled. This is shown in great detail by several authors for amorphous solid targets<sup>4-12</sup> as well as for gaseous targets.<sup>13,16</sup>

(2) For  $0.1 \lesssim \tau \lesssim 0.4$ , the scaling properties are still valid, whereas the absolute width of the distributions are no longer in agreement with the results calculated from TF or LJ potentials. However, the width and shape of the distributions are well described by the empirical power-law potential found by Sidenius and Andersen.<sup>15</sup> For the "effective" collisions,  $2 \times 10^{-2} \lesssim t^{1/2} \lesssim 10^{-1}$ .

(3) When  $\tau \lesssim 0.1$ , the effective  $t^{1/2}$  values are smaller than  $2 \times 10^{-2}$ . Here, according to the present results, significant deviations from the scaling laws occur. This means that the distributions in reduced parameters are not given as a function of  $\tau$  only but are, in addition, dependent on  $Z_1$ ,  $Z_2$ , and  $E$ . Thus it is found that the width of the distributions (and, to a lesser extent, the shape) oscillates as a function of  $Z_1$ . For xenon targets, the width exhibits maxima for  $Z_1 \approx 15$  and 38 and minima for  $Z_1 = 8, 29, \text{ and } 47$ . For  $\tau \approx 0.033$  and

50-keV energy, the amplitude is approximately 40% around  $Z_1 \approx 29$ . The existence of  $Z_2$  oscillations is indicated by measurements performed recently<sup>21</sup> of lateral scattering of 50-keV Pb ions on several different gas targets. The directly measured HWHM's are not strictly proportional to  $E^{-1}$  [Eq. (18)] but to  $E^{-(1+\gamma)}$ . This means that the scattering is not caused by an energy-independent potential.  $\gamma$  has been found to be positive for a  $Z_1$  value corresponding to a maximum, whereas a negative  $\gamma$  value was found near a minimum in the  $Z_1$  oscillations. For the multiple-scattering distributions investigated in the present work, it is still possible to describe both their shape and  $\tau$  dependence by using suitable power-law potentials, but these have to be selected individually for the actual values of  $Z_1$ ,  $Z_2$ , and  $E$  in question. For  $E = 50$  keV, power-law-potential parameters such as those given in Table I can be used to extract theoretical results from Refs. 3 and 14.

It is worth noticing that the observed  $\gamma$  values of the energy dependence suggest that at ion energies greater than those investigated here the oscillations may vanish, thereby restoring the  $E$ ,  $Z_1$ , and  $Z_2$  scaling.

In the following, possible mechanisms causing the observed departure from the scaling properties of simple multiple-scattering theory will be discussed. In this connection, we have to account for the observed oscillations.

The first suggestion is that directly through Eq. (21) they should be due to the well-known oscillations in electronic stopping power  $S_e$ . Such oscillations have been found experimentally both for solid targets (see, e.g., Refs. 22–24) and for gas targets (see, e.g., Ref. 25), and they have been explained by means of various theoretical models (see Refs. 26–28).  $S_e$  oscillates with  $Z_1$  with a relative amplitude that decreases for increasing ion energy, and extrema have been found by Kanaya and Hojou<sup>28</sup> at 29 and 47 (minima) and at 38 (maximum). These characteristics are valid also for our oscillations, but these cannot be explained by  $S_e$  through Eq. (21), since the mean value of  $\frac{1}{2}\Delta E_e$  in our case is  $\approx 1\%$  of the ion energy.

Here we are going to present two different (though not mutually independent) possible mechanisms:

(1) The effects might be ascribed to the characteristics of the elastic differential-scattering cross section [Eq. (1)] between the ions and the target atoms. According to Fig. 1, the interesting range is  $6 \times 10^{-5} \leq t^{1/2} \leq 2 \times 10^{-2}$  since the oscillations are observed at  $0.01 \leq \tau \leq 0.1$ . This corresponds to an impact-parameter interval of  $4a \leq p \leq 17a$ . In this model,  $f(t^{1/2})$ , integrated in a suitable way [see Ref. 3, Eqs. (8) and (9)] over the important  $t^{1/2}$  interval, must oscillate as a function of  $Z_1$  and

$Z_2$ . Measurements performed by Loftager and Clausen<sup>29</sup> show anomalies in  $f(t^{1/2})$  at small  $t^{1/2}$  values, and these might give rise to an oscillatory behavior of the multiple-scattering distributions. Because of the close connection between elastic angular deflection and elastic energy loss, the elastic-stopping cross section  $S_n$  should also oscillate with  $Z_1$  when only weak collisions are present. This is actually observed by Nelson<sup>30</sup> for channeled particles where the impact parameters are comparable to those in question here. Högberg and Skoog<sup>31</sup> also searched for  $Z_1$  oscillations in  $S_n$  but found none. As their effective collisions have impact parameters much smaller than those investigated here, this is not in contradiction to this explanation.

If multiple scattering can be described solely through  $f(t^{1/2})$  for our  $\tau$  range, it is possible to deduce information on  $f(t^{1/2})$  from the experimental results of Fig. 5. In our range of  $t^{1/2}$  values, such information is difficult to obtain by other experimental techniques.<sup>29,32,33</sup> We can find  $f(t^{1/2})$  averaged over suitable  $t^{1/2}$  intervals and averaged over our  $Z_1$  values for xenon targets and an ion energy of 50 keV. This is done by realizing that besides Eq. (25), the experimental points are also described rather well by a straight line parallel to the LJ curve but located about a factor of 2 higher. The LJ potential is approximated by a power-law potential, where in Eq. (6)  $\lambda_m = 2.92$  and  $m = 0.191$  in our  $t^{1/2}$  interval. According to Ref. 3,  $\bar{\alpha}^2 f_1(\tau, \bar{\alpha})$  is a function of  $\bar{\alpha}^{2m}/C_m \tau$  only, and consequently  $\lambda_m$  is proportional to  $\bar{\rho}_{1/2}^{2m}$ ; we therefore find

$$f(t^{1/2}) = 3.80 (t^{1/2})^{0.618} \quad (29)$$

as an average expression for  $f(t^{1/2})$  for  $0.01 \leq \tau \leq 0.07$ , i.e., for  $6 \times 10^{-5} \leq t^{1/2} \leq 10^{-2}$ .

(2) One is led to another possible explanation of the experimental results by the observation that as a result of the large impact parameters the elastic collisions might be weak enough for scattering on the target electrons to become important. Accordingly, the oscillations might be due to variations in multiple scattering on electrons. An estimate performed by Bonderup<sup>34</sup> indicates that this is indeed an effect of the same order of magnitude as ordinary nuclear multiple scattering at the lowest  $\tau$  values investigated here. Furthermore, the estimate shows that the electron multiple-scattering HWHM  $\bar{\rho}_{1/2,e}$  is approximately proportional to  $S_e^{1/2}$ . In this model, the oscillations of  $\bar{\rho}_{1/2}$  (and  $\bar{\alpha}_{1/2}$ ) should, consequently, be closely related to the  $S_e$  oscillations. This is actually the case (see above). A weakness of this interpretation arises from the fact that Bonderup predicts  $\bar{\rho}_{1/2}$  to be proportional to  $\tau$  in the power 1.5, whereas we observe a power of  $\sim 3.5$ .

The two models sketched here are not independent but rather are two different ways of approaching an explanation of the experimental results. This is due to the fact that we are dealing with collisions where it is probably not possible to strictly distinguish between elastic nuclear collisions and inelastic electronic collisions. But the two explanations not only create the possibility of obtaining a better understanding of multiple scattering at very small target thicknesses; they also indicate methods for a quantitative theoretical investigation.

In this work, we have concentrated on targets where the atoms are randomly distributed. It has been shown<sup>10</sup> that the spatial correlation between the atoms in polycrystalline solid targets can drastically reduce multiple scattering. It was recently found<sup>21</sup> that at target thicknesses as small as those investigated here, even the weak spatial correlations existing in molecular gas targets can cause large deviations from multiple scattering on monatomic gases.

#### VII. CONCLUSION

For the multiple-scattering distributions investigated here, where the ion energy is in the keV

range, deviations from the basic scaling with atomic number and energy inherent in current multiple-scattering theory is found for  $\tau \approx 0.1$ .  $Z_1$  oscillations in the width of the distributions at fixed  $\tau$  are observed, and the widths are not strictly proportional to the reciprocal energy. Nevertheless, it is still possible to describe the  $\tau$  dependence and the shape of the distributions, given  $Z_1$ ,  $Z_2$ , and  $E$ , by using the results of Refs. 3 and 14 for suitable power-law potentials.

The observed oscillations may be explained as stemming from either an oscillatory behavior of the interatomic potential at large impact parameters or multiple scattering on the target electrons being superimposed on the nuclear multiple scattering.

#### ACKNOWLEDGMENTS

Many fruitful discussions with N. Andersen, G. Sidenius, and P. Sigmund are gratefully acknowledged. We also wish to thank H. H. Andersen, E. Bonderup, and J. Lindhard for their inspiring interest in the project.

- 
- <sup>1</sup>G. Molière, *Z. Naturforsch. A* **3**, 78 (1948).  
<sup>2</sup>L. Meyer, *Phys. Status Solidi B* **44**, 253 (1971).  
<sup>3</sup>P. Sigmund and K. B. Winterbon, *Nucl. Instrum. Methods* **119**, 541 (1974).  
<sup>4</sup>G. Högberg, H. Nordén, and H. G. Berry, *Nucl. Instrum. Methods* **90**, 283 (1970).  
<sup>5</sup>S. Schwabe and R. Stolle, *Phys. Status Solidi B* **47**, 111 (1971).  
<sup>6</sup>H. H. Andersen and J. Böttiger, *Phys. Rev. B* **4**, 7 (1971).  
<sup>7</sup>F. Bernhard, P. Krygel, R. Manns, and S. Schwabe, *Radiat. Effects* **13**, 249 (1972).  
<sup>8</sup>H. H. Andersen, J. Böttiger, and H. Knudsen, *Radiat. Effects* **13**, 203 (1972).  
<sup>9</sup>H. G. Schäffler, Max-Planck-Institut für Plasmaphysik Garching Report No. IPP 9/14, 1973 (unpublished).  
<sup>10</sup>H. H. Andersen, J. Böttiger, H. Knudsen, P. Möller Petersen, and T. Wohlenberg, *Phys. Rev. A* **10**, 1568 (1974).  
<sup>11</sup>G. Spahn and K. O. Groeneveld, *Nucl. Instrum. Methods* **123**, 425 (1975).  
<sup>12</sup>B. W. Hooton, J. M. Freeman, and P. P. Kane, *Nucl. Instrum. Methods* **124**, 29 (1975).  
<sup>13</sup>B. Efken, D. Hahn, D. Hilscher, and G. Wüstefeld, *Nucl. Instrum. Methods* **129**, 227 (1975).  
<sup>14</sup>A. D. Marwick and P. Sigmund, *Nucl. Instrum. Methods* **126**, 317 (1975).  
<sup>15</sup>G. Sidenius and N. Andersen, *Nucl. Instrum. Methods* **128**, 271 (1975).  
<sup>16</sup>G. Sidenius and N. Andersen, *Nucl. Instrum. Methods* **131**, 387 (1975).  
<sup>16(a)</sup>This work is part of a more extensive investigation performed in coordination with similar work carried out at the University of Copenhagen (N. Andersen and P. Sigmund, the H. C. Ørsted Institute, and G. Sidenius, the Niels Bohr Institute). Until now, lateral multiple scattering has been investigated for reduced target thicknesses  $0.01 < \tau < 20$ . Its outline has been sketched by N. Andersen, P. Sigmund, J. Heinemeier, P. Hvelplund, H. Knudsen, and G. Sidenius, *Proceedings of the International Conference on Atomic Collisions in Solids*, Amsterdam (1975) (unpublished), and *Nucl. Instrum. Methods* **132**, 703 (1976).  
<sup>17</sup>J. Lindhard, V. Nielsen, and M. Scharff, *K. Dan. Vidensk. Selsk. Mat.-Fys. Medd.* **36**, No. 10 (1968).  
<sup>18</sup>P. Sigmund (private communication).  
<sup>19</sup>P. Hvelplund, E. Laegsgaard, J. Ø. Olsen, and E. H. Pedersen, *Nucl. Instrum. Methods* **90**, 315 (1970).  
<sup>20</sup>J. Lindhard, M. Scharff, and H. E. Schiøtt, *K. Dan. Vidensk. Selsk. Mat.-Fys. Medd.* **33**, No. 14 (1963).  
<sup>21</sup>G. Sidenius, N. Andersen, P. Sigmund, F. Besenbacher, J. Heinemeier, P. Hvelplund, and H. Knudsen, *Nucl. Instrum. Methods* (to be published).  
<sup>22</sup>P. Hvelplund and B. Fastrup, *Phys. Rev.* **165**, 408 (1968).  
<sup>23</sup>J. Böttiger and F. Bason, *Radiat. Effects* **2**, 105 (1969).  
<sup>24</sup>F. H. Eisen, *Can. J. Phys.* **46**, 561 (1968).  
<sup>25</sup>P. Hvelplund, *K. Dan. Vidensk. Selsk. Mat.-Fys. Medd.* **38**, No. 4 (1971).  
<sup>26</sup>S. P. Ali and D. F. Gallaher, *J. Phys. C* **7**, 2434 (1974); J. S. Briggs and A. P. Pathak, *ibid.* **7**, 1929 (1974).  
<sup>27</sup>I. M. Cheshire and J. M. Poate, in *Proceedings of the International Conference on Atomic Collision Phenomena in Solids*, Sussex, Brighton, edited by D. W.

- Palmer, M. W. Thompson, and P. D. Townsend (North-Holland, Amsterdam, 1969), p. 351; C. P. Bhalla, J. N. Bradford, and G. Reese, *ibid.*, p. 361.
- <sup>28</sup>K. Kanaya and K. Hojou, *Jpn. J. Appl. Phys.* 13, 393 (1974).
- <sup>29</sup>P. Loftager and G. Clausen, in *Proceedings of the Sixth International Conference on the Physics of Electronic and Atomic Collisions, Cambridge, Mass., 1969*, edited by I. Amdur (MIT Press, Cambridge, Mass., 1969), p. 518.
- <sup>30</sup>R. S. Nelson, *Phys. Lett.* 28A, 676 (1969).
- <sup>31</sup>G. Högberg and R. Skoog, *Radiat. Effects* 13, 197 (1972).
- <sup>32</sup>H. H. Andersen, J. Böttiger, and H. Knudsen, *Phys. Rev. A* 7, 154 (1973); H. H. Andersen and H. Knudsen, *Phys. Rev. A* 10, 733 (1974).
- <sup>33</sup>H. Knudsen and P. Møller Petersen, *Radiat. Effects* (to be published).
- <sup>34</sup>E. Bonderup (private communication).